Supporting Information

Regulation of Various Photo-active UOP in Polymer Matrix by Tuning Intermolecular Charge Transfer

*Haodong Sun,[a] Xiaoyu Wei,[a] Yunfei He,[a] Wazhang Wu,[a] Zongliang Xie,[a] and Tao Yu[a] [b,] **

[a] Frontiers Science Center for Flexible Electronics (FSCFE), Shaanxi Institute of Flexible Electronics (SIFE) & Shaanxi Institute of Biomedical Materials and Engineering (SIBME), Northwestern Polytechnical University (NPU), 127 West Youyi Road, Xi'an 710072, China.

[b] Key Laboratory of Flexible Electronics of Zhejiang Province, Ningbo Institute of Northwestern Polytechnical University, 218 Qingyi Road, Ningbo 315103, China

E-mail: iamtyu@nwpu.edu.cn;

1 Regents and materials

3-(4,4,5,5-tetramethyl-1,3,2-dioxaborolan-2-yl)-9H-carbazole, 4-bromobenzonitrile, 4-bromophthalonitrile, and potassium carbonate (K_2CO_3) were purchased from Shanghai Energy-Chemical Co. Ltd. and used without any further purification. All reagents were purchased from Sigma-Aldrich. Tetrakis(triphenylphosphine)palladium ($Pd(PPh_3)_4$) was synthesized by our group. Poly(methyl methacrylate) (PMMA, average molecular weight ~200,000) and poly(vinyl alcohol) (PVA, average molecular weight ~105,000, alcoholysis degree 98.0 ~ 99.0 mol%) were also purchased from Shanghai Energy-Chemical Co. Ltd.

2 Synthesis and Characterization of Compounds

The synthetic routes of the target compounds were shown below. The final compounds were characterized by ^1H NMR and high-resolution ESI mass spectrometry. The purity of the final compounds was monitored by high-performance liquid chromatography (HPLC).

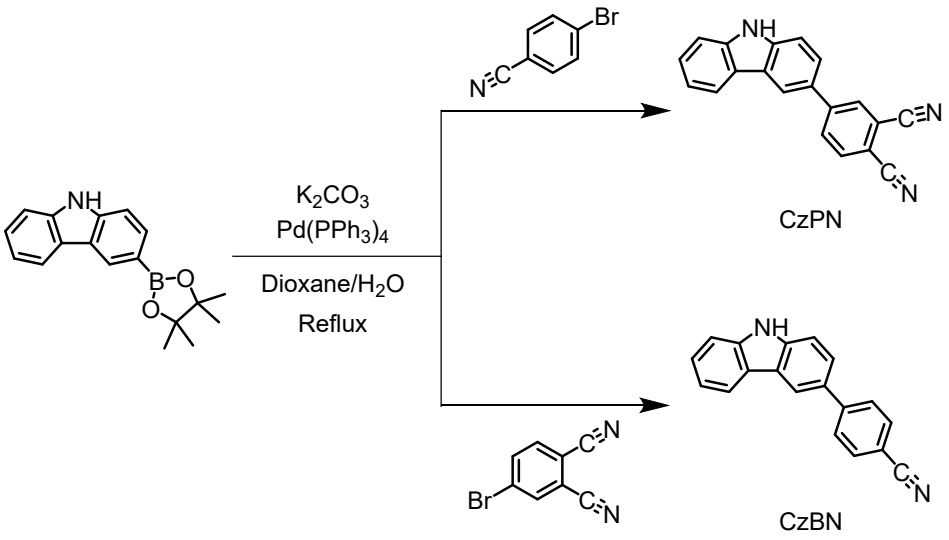

Scheme S1 Synthetic routes for CzBN and CzPN.

Synthesis of 4-(9H-carbazol-3-yl)phthalonitrile (CzPN)

3-(4,4,5,5-tetramethyl-1,3,2-dioxaborolan-2-yl)-9H-carbazole (0.80 g, 3.86 mmol), 4-bromophthalonitrile and dioxane (1.13 g, 3.86 mmol), K_2CO_3 (3.20g, 23.19 mmol), $Pd(PPh_3)_4$ (0.09 g, 0.77 mmol) mixed solution of dioxane (21 mL) and deionized water (7 mL) were mixed in a dried flask under argon atmosphere. The mixture was stirred at 100 °C for 18 h. After cooling to room temperature, the mixed solution was distilled out to obtain dry solid. The dry solid was dissolved in dichloromethane (DCM) and washed with brine. After removal of the solvents of the organic layer, the crude products were purified by silica-gel chromatography with DCM/n-hexane (2/1, v/v) to give CzPN (0.48 g, 42.08 %).

^{1}H NMR (500 MHz, $(CD_3)_2SO$, 298 K), (TMS, ppm): δ = 11.53 (s, 1H), 8.76 (s, 1H), 8.36 (d, 1H), 8.26 – 8.18 (m, 2H), 7.92 (d, 1H), 7.62 (d, 1H), 7.53 (d, 1H), 7.44 (t, 1H), 7.24 (t, 1H).

High-Resolution ESI-MS: m/z found: 316.0845 [Na^+], calcd for $C_{20}H_{11}N_3Na^+$, 316.0845.

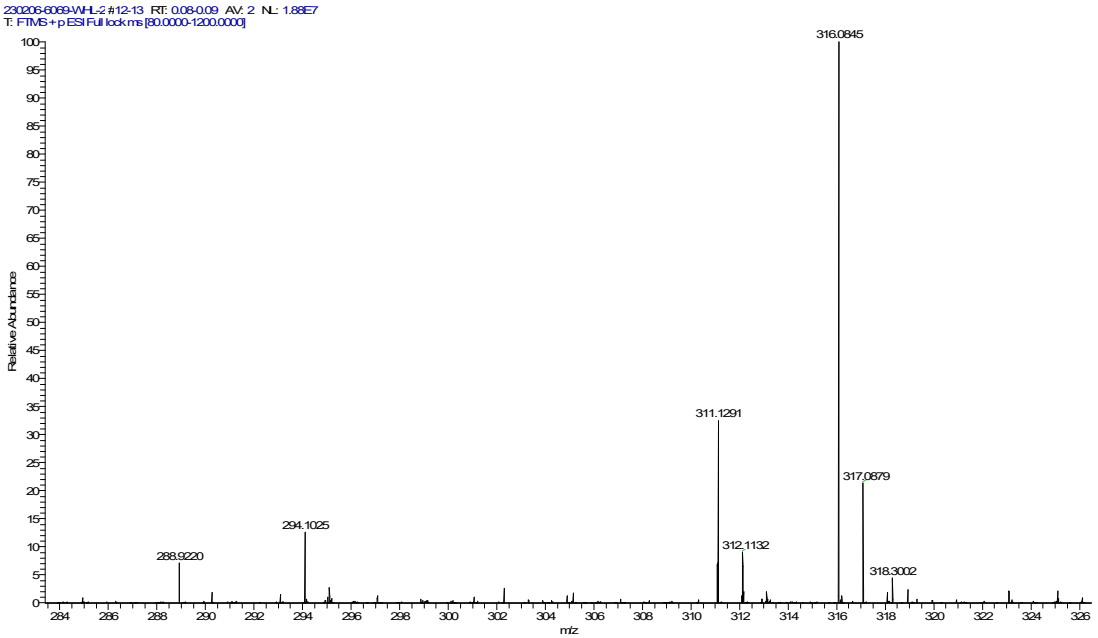

Figure S1. High-Resolution ESI mass spectrum of CzPN.

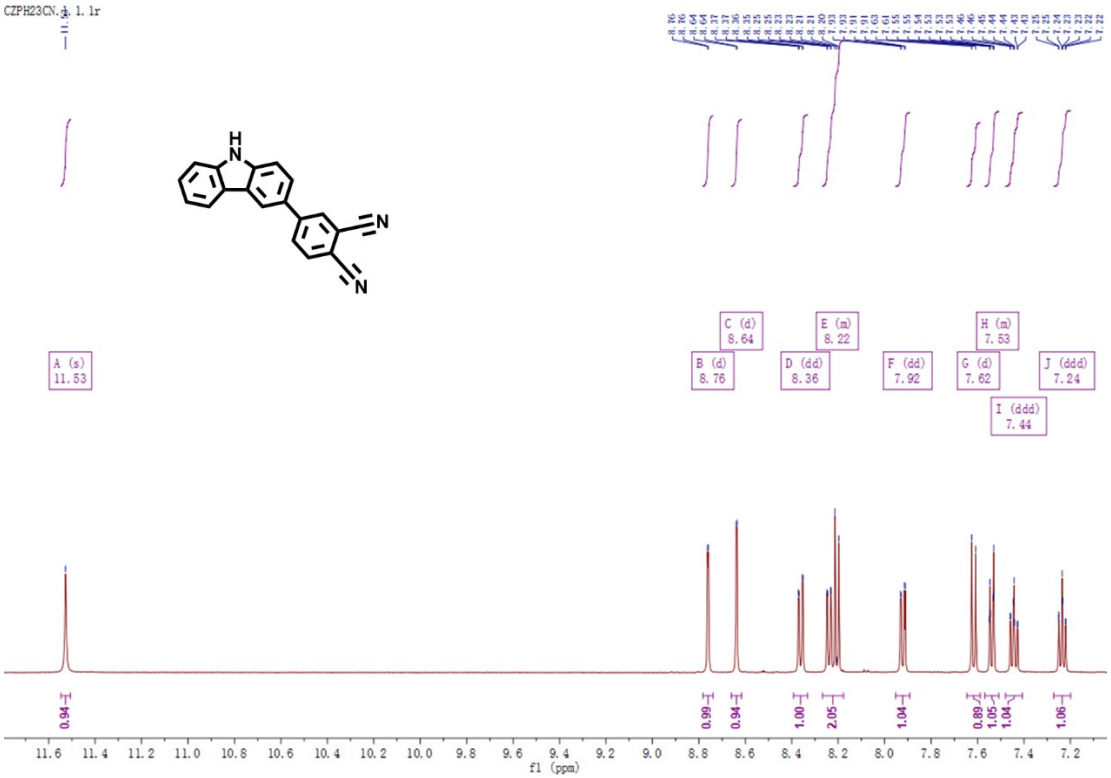

Figure S2. ^{1}H NMR spectrum (500 MHz) of **CzPN** in $(CD_3)_2SO$.

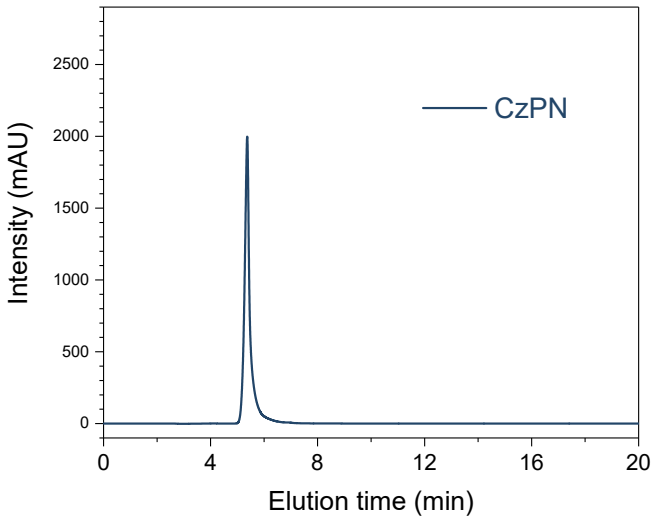

Figure S3. HPLC spectrum of CzPN recorded at 254 nm with acetonitrile:water as eluent in ratios of 70:30 (v/v).

Synthesis of 4-(9H-carbazol-3-yl)benzonitrile (CzBN)

CzBN was synthesized using the same method as CzPN. CzBN powder in white was obtained (0.33 g, 45.32 %). ^{1}H NMR (500 MHz, $CDCl_3$, 298 K), (TMS, ppm): δ = 8.30 (s, 1H), 8.18 (s, 1H), 8.13 (d, *J* = 7.9 Hz, 1H), 7.80 (d, 2H), 7.74 (d, *J* = 8.3 Hz, 2H), 7.66 (d, *J* = 8.4 Hz, 1H), 7.52 (d, *J* = 8.4 Hz, 1H), 7.49 – 7.45 (m, 2H), 7.29 (ddd, *J* = 8.0, 5.2, 2.9 Hz, 1H).

High-Resolution ESI-MS: m/z found: 291.0893 [Na^+], calcd for $C_{19}H_{12}N_2Na^+$, 291.0893.

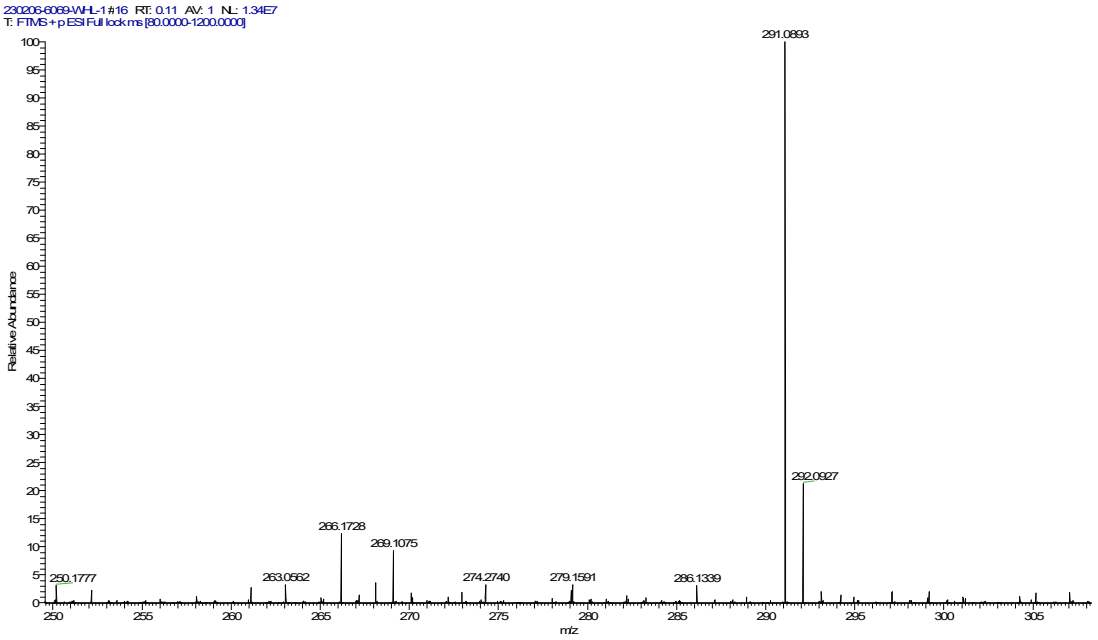

Figure S4. High-Resolution ESI mass spectrum of CzBN.

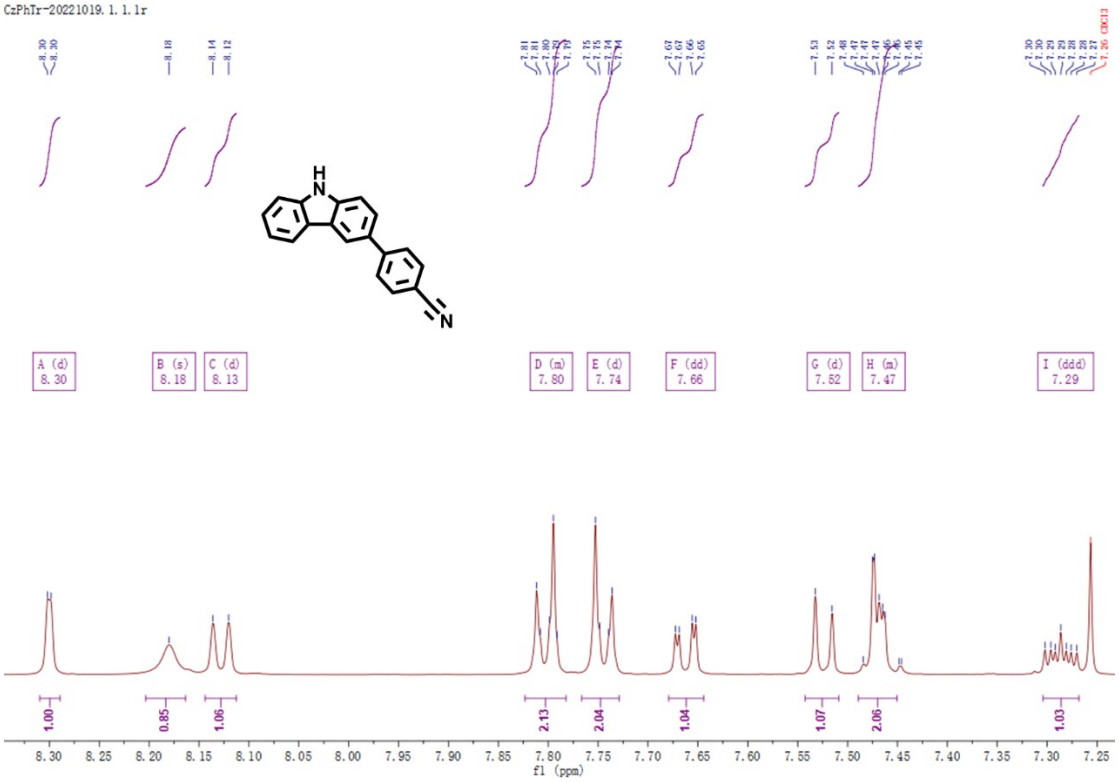

Figure S5. ^{1}H NMR spectrum (500 MHz) of **CzBN** in $CDCl_3$.

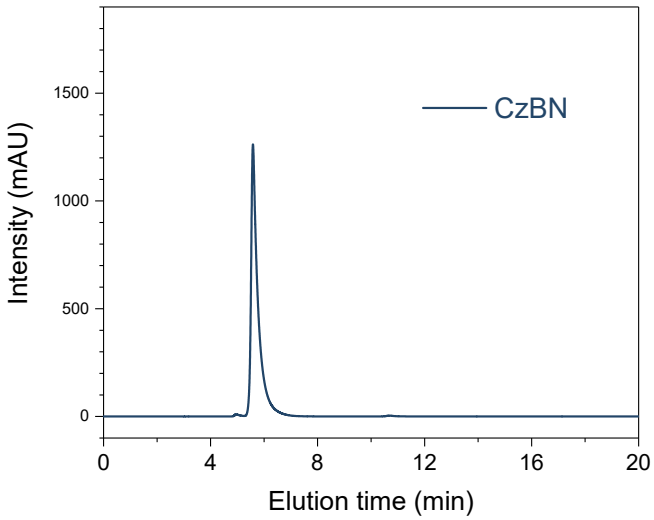

Figure S6. HPLC spectrum of CzBN recorded at 254 nm with acetonitrile:water as eluent in ratios of 70:30 (v/v).

3 Procedure of the film fabrication

PMMA solution (100mg/mL): PMMA (2 g) and tetrahydrofuran (THF, 20 mL) solvent were mixed in a flask and stirred for 24 hours at room temperature until the PMMA particles completely dissolved. The clear PMMA/THF solution was used for the subsequent film fabrication.

PVA solution (50mg/mL): PVA (1 g) and deionized water (20 mL) were mixed in a flask and stirred for 24 hours at 95 °C to obtain clear PVA/H_2O solutions. The clear PMMA/THF solution was used for the subsequent film fabrication.

CzPN@PMMA or CzBN@PMMA films (1 wt%): Mixed CzPN or CzBN (5 mg) in PMMA/THF solution (5 mL) at a vessel. The mixture was ultrasonicated for 1 h and then the mixture (1 mL) was dropped onto a glass substrate (3 cm* 3 cm). After evaporation of the solvent, the films were placed in a drying oven at 70 °C for 6 h. The films of CzPN@PMMA or CzBN@PMMA with different doping concentration (0.1

wt%, 0.5 wt%, and 5 wt%) were fabricated by changing the mass of CzPN or CzBN (0.5 mg, 2.5 mg, 25 mg) in PMMA/THF solution (5 mL).

CzPN@PVA or CzBN@PVA films (1 wt%): CzPN or CzBN (5 mg), dimethyl sulfoxide (5 mL), and PVA/H_2O solutions (10 mL) were mixed at a vessel. The mixture (1 mL) was dropped onto a glass substrate (3 cm* 3 cm). The films were placed in a drying oven at 90 °C for 24 h. The fabrication of CzPN@PMMA or CzBN@PMMA films with different doping concentration (0.1 wt%, 0.5 wt%, and 5 wt%) was the same as CzPN@PMMA or CzBN@PMMA.

4 Physical measurements and instrumentations

^{1}H NMR spectra were performed with a Bruker AVANCE NEO 500 Nuclear Magnetic Resonance Spectrometer (NMRS, 500 MHz) using chloroform-*d* ($CDCl_3$) and dimethyl sulfoxide-d_6 ($(CD_3)_2SO$). The chemical shift references were as follows: (^{1}H) chloroform-*d*, 7.26 ppm, (^{1}H) dimethyl sulfoxide-d_6, 2.50 ppm, and tetramethylsilane (TMS) as the internal standard. High performance liquid chromatography (HPLC) was performed on an UltiMate 3000. High-Resolution ESI mass spectra (HRMS) were collected from Thermo Scientific Q-Exactive spectrometer. The UV-visible absorption spectra of dilute solution were performed on Hitachi U-3900. The steady-state PL spectra of dilute solution were tested on Hitachi F7100. The PL spectra, delayed spectra, time-resolved PL-decay curves, and absolute photoluminescence quantum yield (PLQY) and were tested on Edinburgh steady-transient fluorescence spectrometer (FLS-1000) equipped with an integrating-sphere accessory. The transient PL decay

image and part of delayed spectra were recorded on a Shimadzu RF-5301 PC spectrometer or an Ocean Optics Spectrometer (QE 65Pro) with 365nm Rhinospectrum RhinoLED as the excitation source. Powder X-ray diffraction (XRD) were performed on Bruker D8 Advance at 298 K. Differential scanning calorimetry (DSC) was performed on NETZSCH DSC 214. The thickness of the polymer films was tested on YongXin NIB 610 (Guona Chenyu Technology Co., Ltd). Optical photographs and videos of the phosphorescent films were shot by a Sony LICE-6400M camera.

5 Theoretical calculations

The molecular geometries of CzBN and CzPN at ground state were optimized via the density functional theory (DFT) method at the B3LYP/6-311G* level in Gaussian 09 program.[1, 2] On that basis, the electronic properties of excited singlet (S_n) and triplet states (T_n) were examined using time-dependent density functional theory (TD-DFT) at the B3LYP/6-311G* level. In this article, energy levels of the possible T_n states were considered to lie within the range of the $E_{S1} \pm 0.3$ eV.[3] Spin-orbital couplings (SOC) matrix elements between the singlet and triplet excited states were calculated via ORCA (program vision 4.2.1) based on B3LYP/G 6-311G*.[4] Natural transition orbital (NTO) analysis was extracted based on TD-DFT result, analyzed by Multiwfn 3.8 and visualized via Visual Molecular Dynamics (VMD) software (version 1.9.3).[5, 6]

6 Photophysical properties and spectra

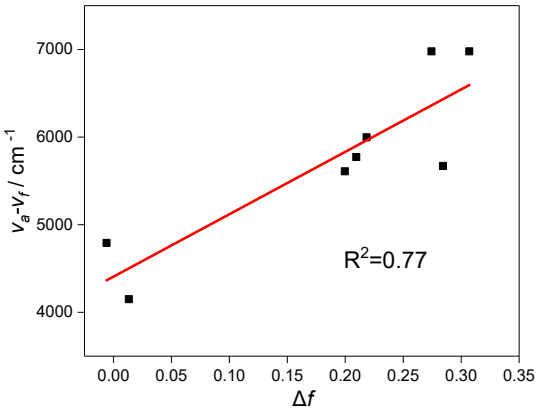

Figure S7 Lippert-Mataga of CzBN in different solvents with increasing polarity.

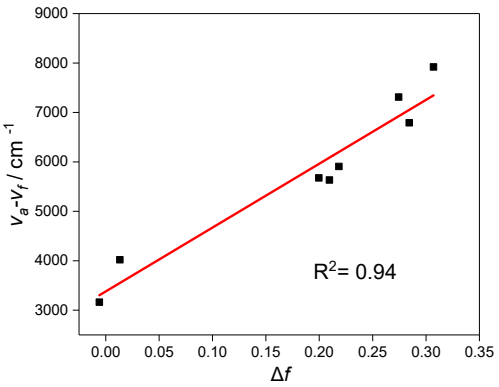

Figure S8 Lippert-Mataga of CzPN in different solvents with increasing polarity.

Table S1 The PLQYs for **CzBN** and **CzPN** in different solutions.

CzBN in different solutions	QuantumYield (%)	CzPN in different solutions	QuantumYield (%)
n-Hexane	42.7	n-Hexane	44.2
Toluene	96.8	Toluene	76.5
Tetrahydrofuran	96.1	Tetrahydrofuran	84.6
Dichloromethane	81.0	Dichloromethane	92.1
Ethyl Acetate	78.5	Ethyl Acetate	81.1
Acetone	62.0	Acetone	71.7
Acetonitrile	83.5	Acetonitrile	61.7
N,N-Dimethylformamide	87.5	N,N-Dimethylformamide	54.4

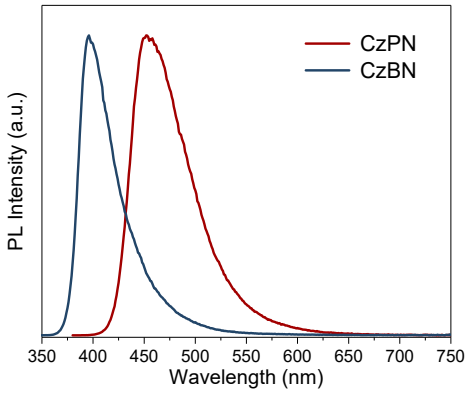

Figure S9 Steady-state PL spectra of crystalline CzBN (blue, λ_{ex} = 330 nm) and CzPN (red, λ_{ex} = 365 nm).

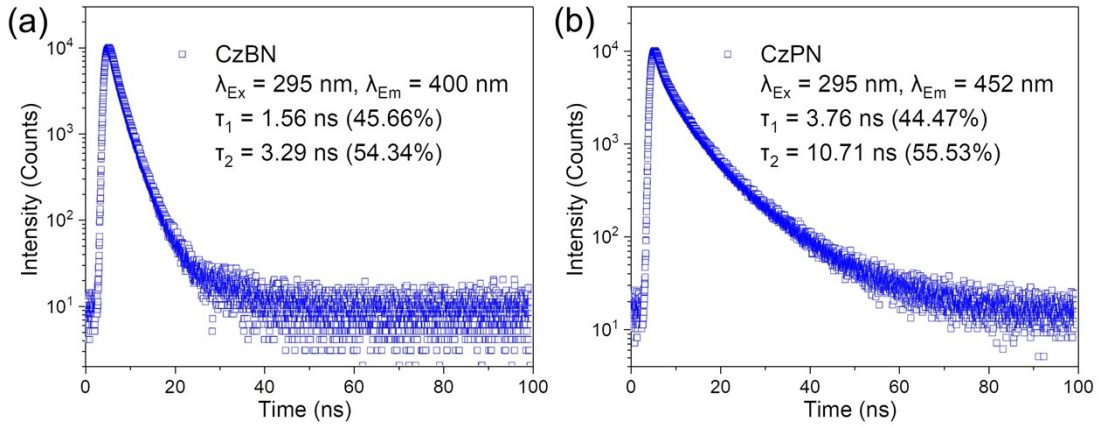

Figure S10 Time-resolved PL decay curves of (a) CzBN and (b) CzPN.

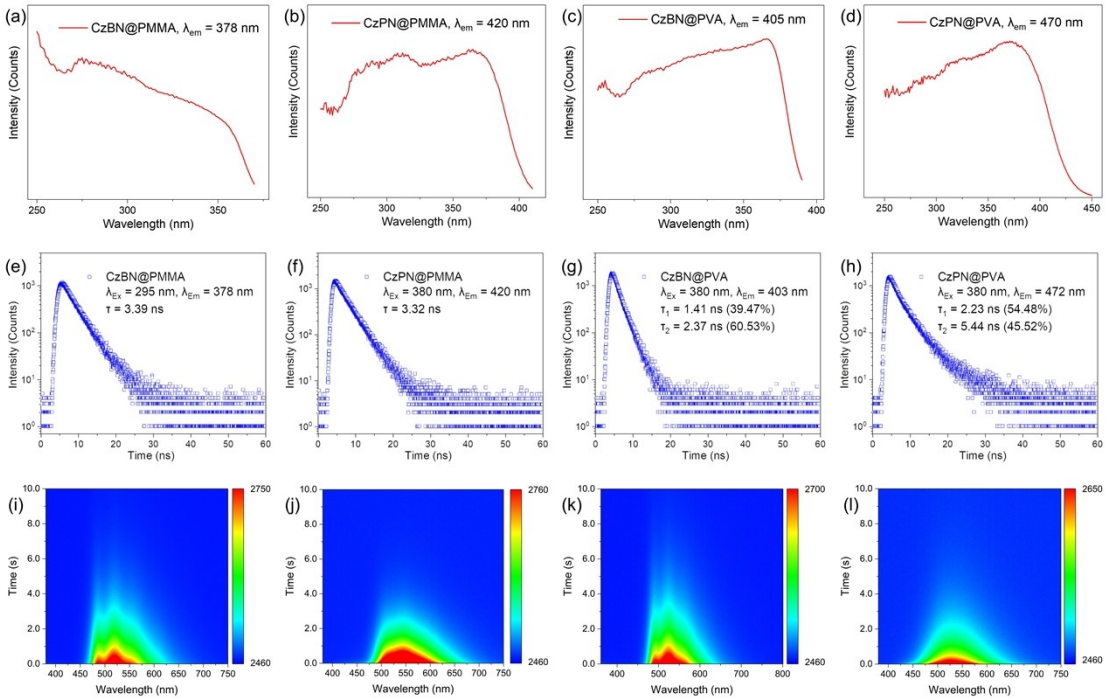

Figure S11 Photophysical properties of CzBN@PMMA, CzPN@PMMA, CzBN@PVA and CzPN@PVA films. (a), (b), (c) and (d) were the excitation spectra of the polymer films. (e), (f), (g) and (h) were the time-resolved decay curves at fluorescent emission peaks of the polymer films. (i), (j), (h) and (d) were the transient PL decay image (delay 8 ms) of CzBN@PMMA, CzPN@PMMA, CzBN@PVA and CzPN@PVA films, respectively.

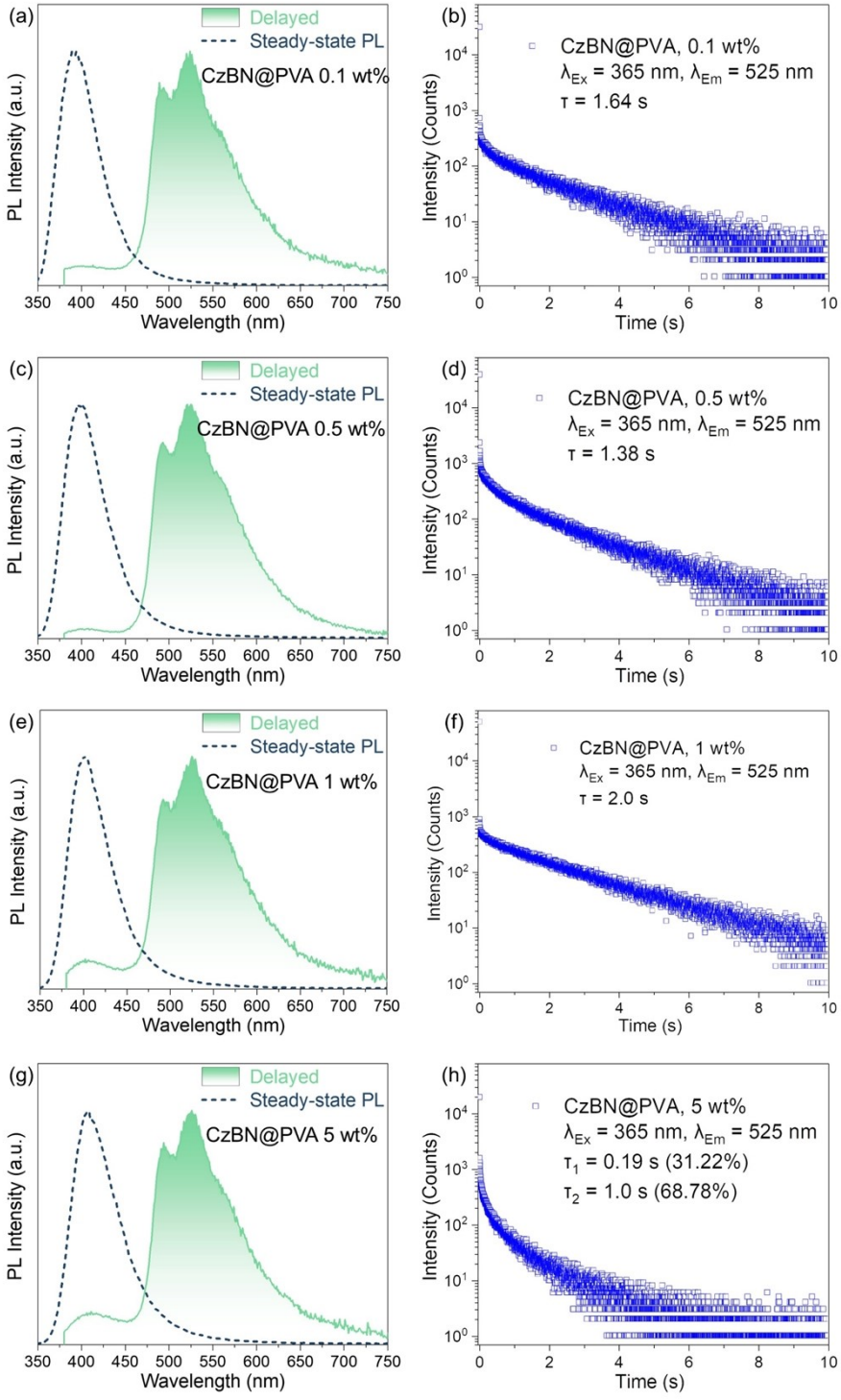

Figure S12 RTP performance of CzBN@PVA films about different doping concentrations (0.1 wt%, 0.5 wt%, 1 wt%and 5 wt%). (a), (c), (d), and (g) were the normalized steady-state PL (blue dash) and delayed spectra (green, delay 8 ms) of CzBN@PVA films about different doping concentrations, respectively. (b), (d), (f), and

(h) were the corresponding time-resolved decay curves.

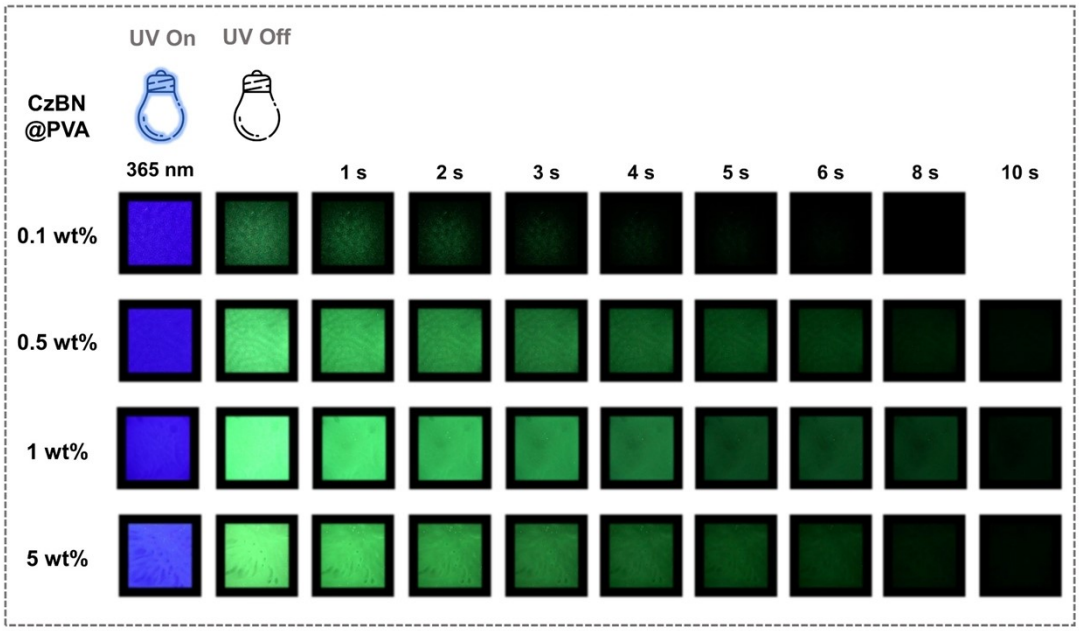

Figure S13 Photographs of CzBN@PVA films about different doping concentrations (0.1 wt%, 0.5 wt%, 1 wt%and 5 wt%) under and after the UV-365 nm excitation.

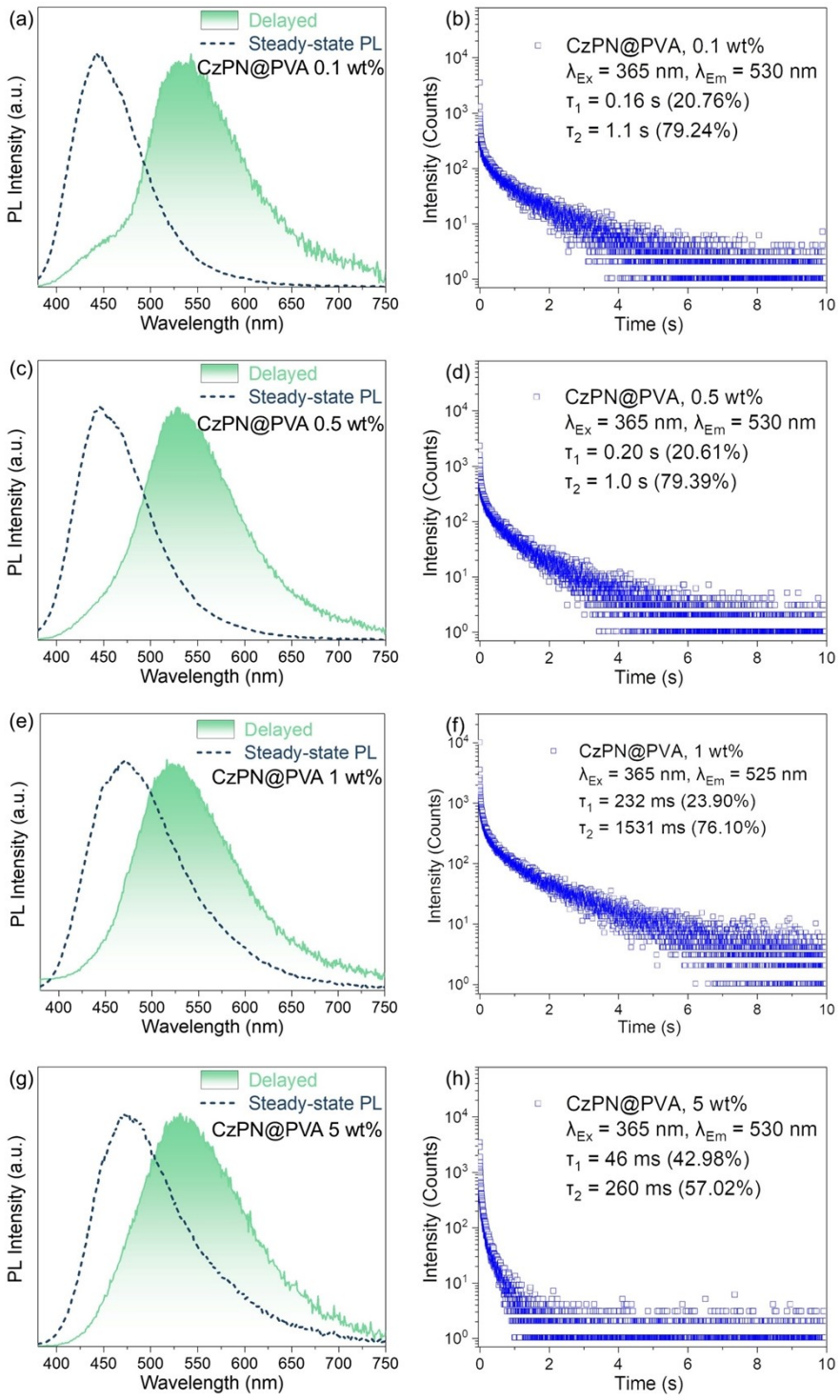

Figure S14 RTP performance of CzPN@PVA films about different doping concentrations (0.1 wt%, 0.5 wt%, 1 wt%and 5 wt%). (a), (c), (d), and (g) were the normalized steady-state PL (blue dash) and delayed spectra (green, delay 8 ms) of CzPN@PVA films about different doping concentrations, respectively. (b), (d), (f), and

(h) were the corresponding time-resolved decay curves.

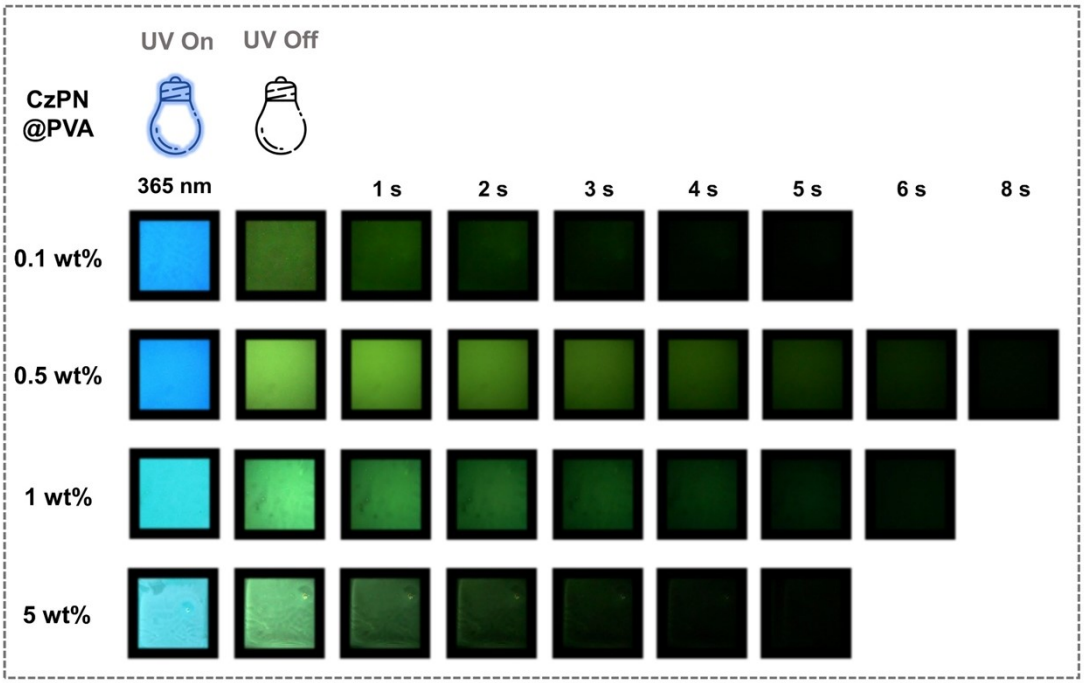

Figure S15 Photographs of CzPN@PVA films about different doping concentrations (0.1 wt%, 0.5 wt%, 1 wt%and 5 wt%) under and after the UV-365 nm excitation.

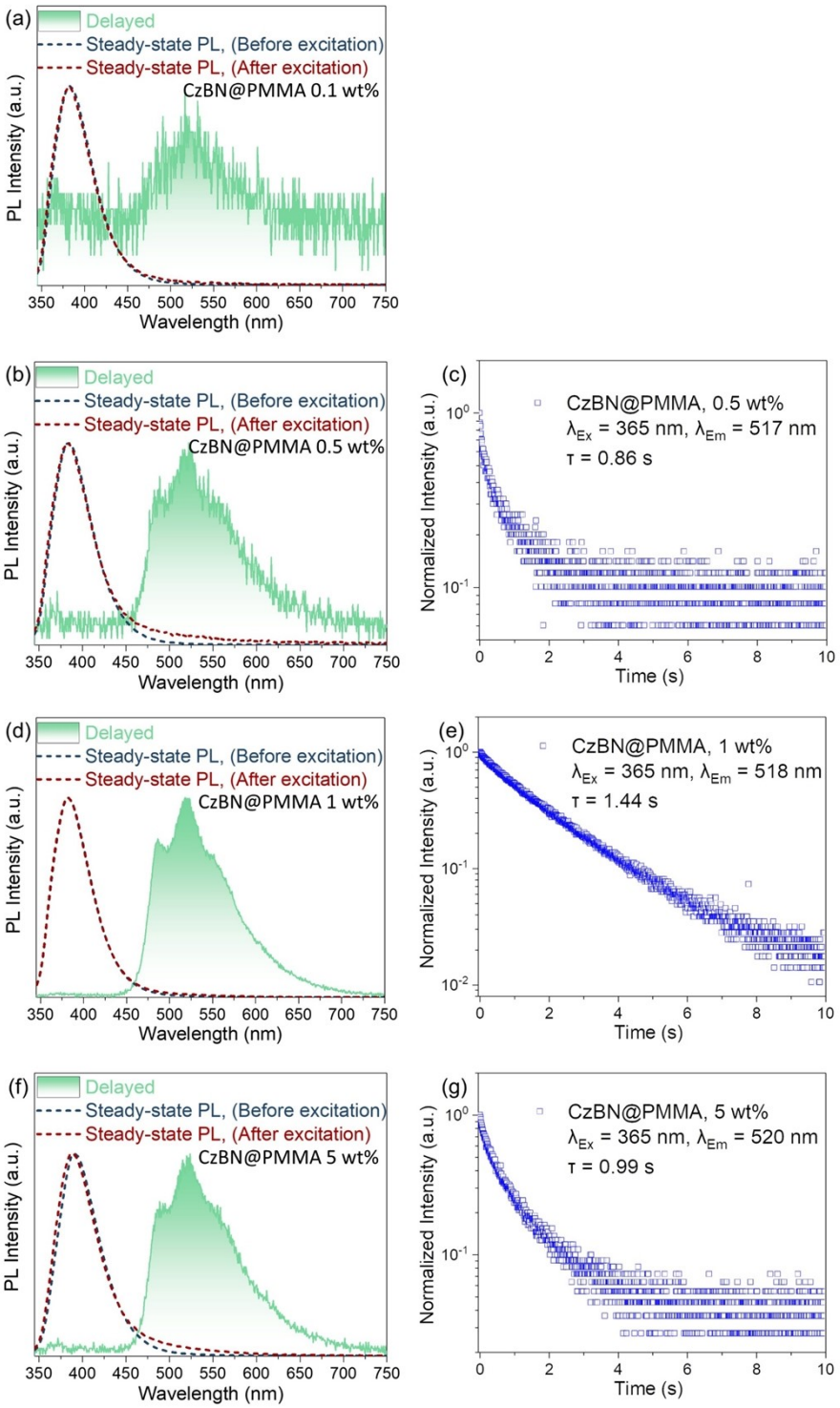

Figure S16 RTP performance of CzBN@PMMA films about different doping concentrations (0.1 wt%, 0.5 wt%, 1 wt%and 5 wt%). (a), (b), (d), and (f) were the normalized steady-state PL before (blue dash) and after (red dash) UV induced process, and delayed spectra (green, delay 8 ms) of CzBN@PMMA films about different doping

concentrations, respectively. (c), (e), and (g) were the corresponding time-resolved decay curves, which recorded on Ocean Optics Spectrometer (QE 65Pro). The RTP emission of CzBN@PMMA films with a doping concentration of 0.1 wt% were hard to observe even after prolonged irradiation.

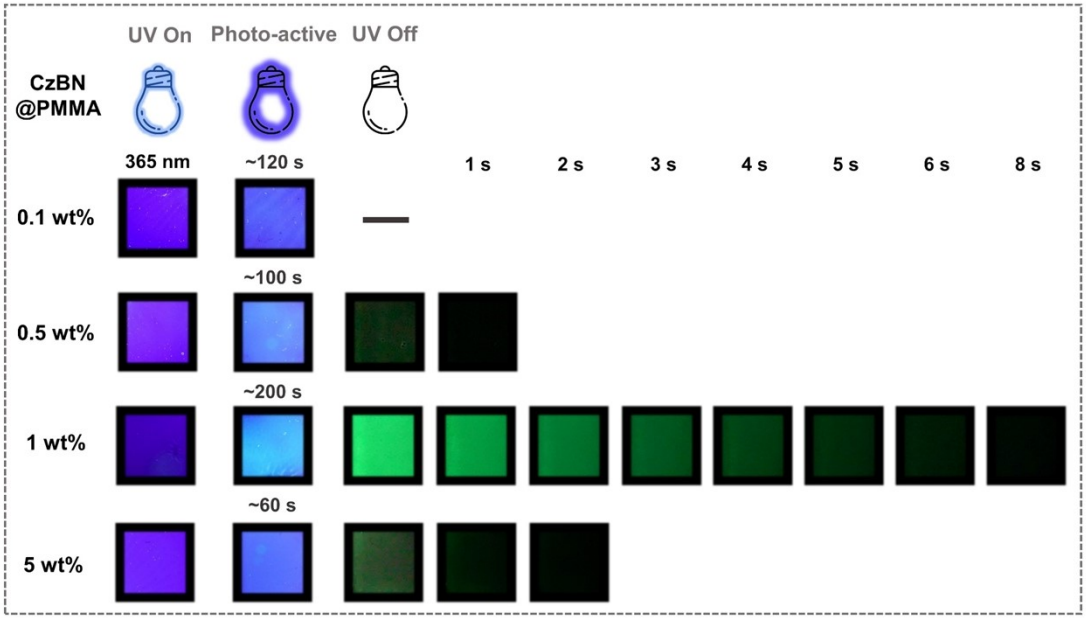

Figure S17 Photographs of CzBN@PMMA films about different doping concentrations (0.1 wt%, 0.5 wt%, 1 wt%and 5 wt%) under and after the UV-365 nm excitation.

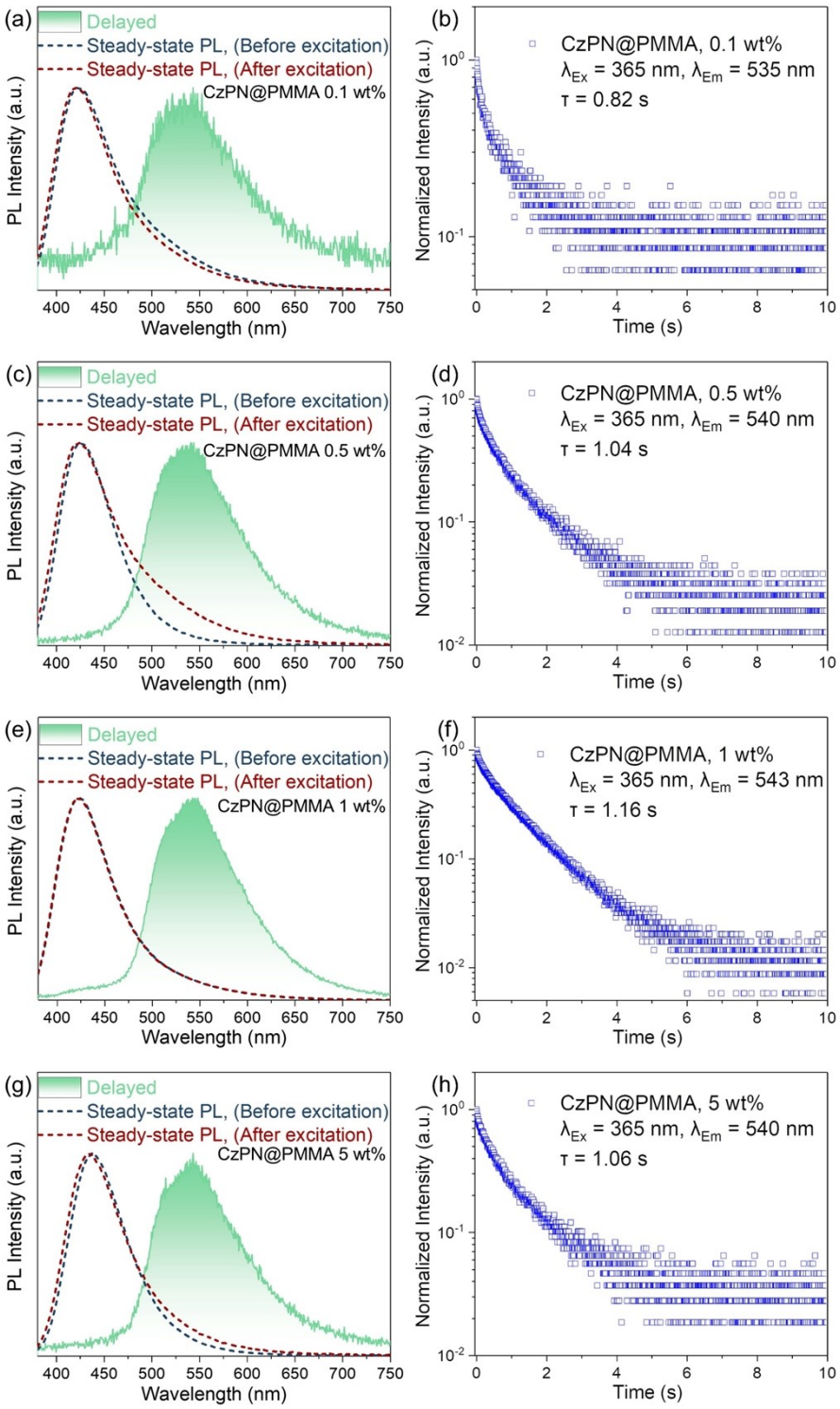

Figure S18 RTP performance of CzPN@PMMA films about different doping concentrations (0.1 wt%, 0.5 wt%, 1 wt%and 5 wt%). (a), (b), (d), and (f) were the normalized steady-state PL before (blue dash) and after (red dash) UV induced process, and delayed spectra (green, delay 8 ms) of CzPN@PMMA films about different doping

concentrations, respectively. (c), (e), and (g) were the corresponding time-resolved decay curves, which recorded on Ocean Optics Spectrometer (QE 65Pro).

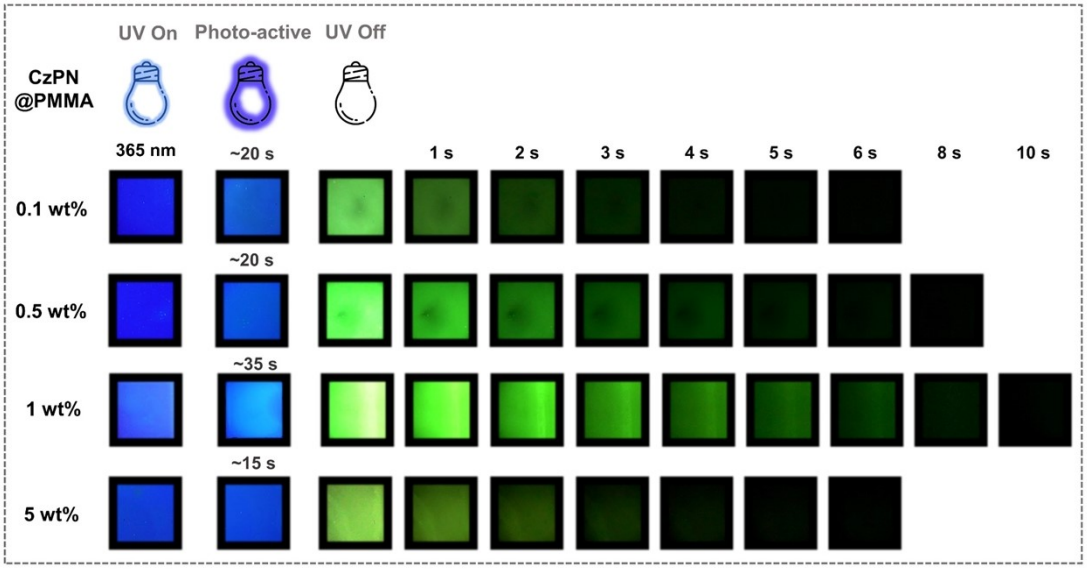

Figure S19 Photographs of CzPN@PMMA films about different doping concentrations (0.1 wt%, 0.5 wt%, 1 wt%and 5 wt%) under and after the UV-365 nm excitation.

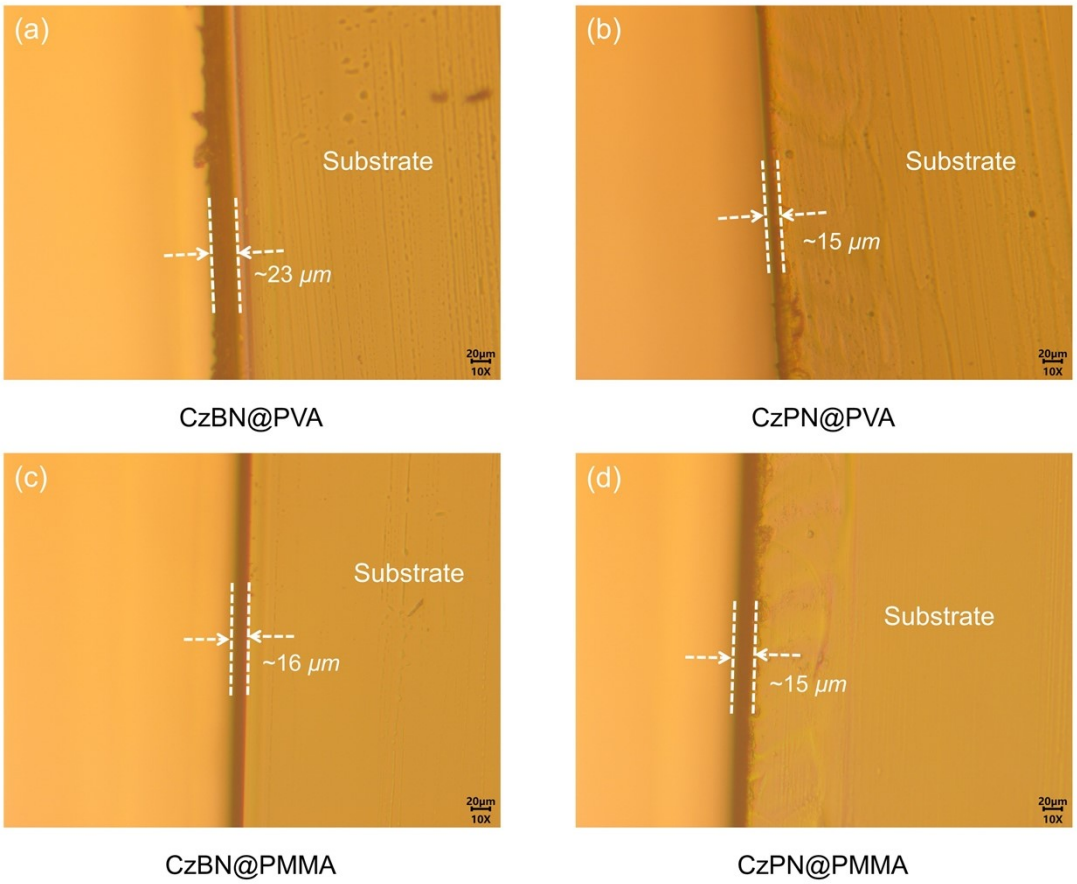

Figure S20. Microscopic images of the polymer films and glass substrate. The thickness of the prepared films was marked in pictures.

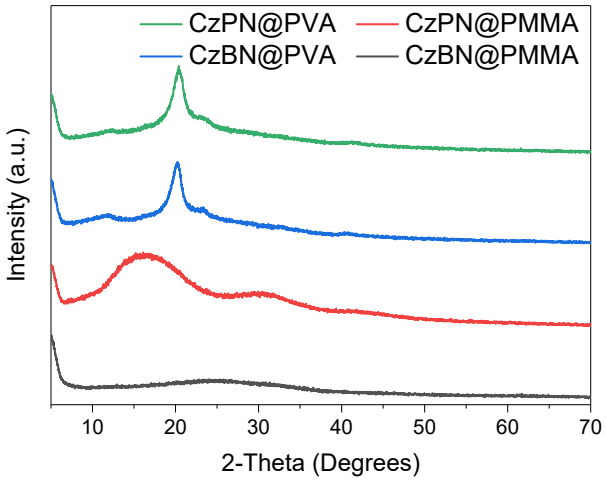

Figure S21 The XRD patterns of CzPN@PVA, CzBN@PVA, CzPN@PMMA, and CzBN@PMMA films. The doping concentration of the films was 1 wt%.

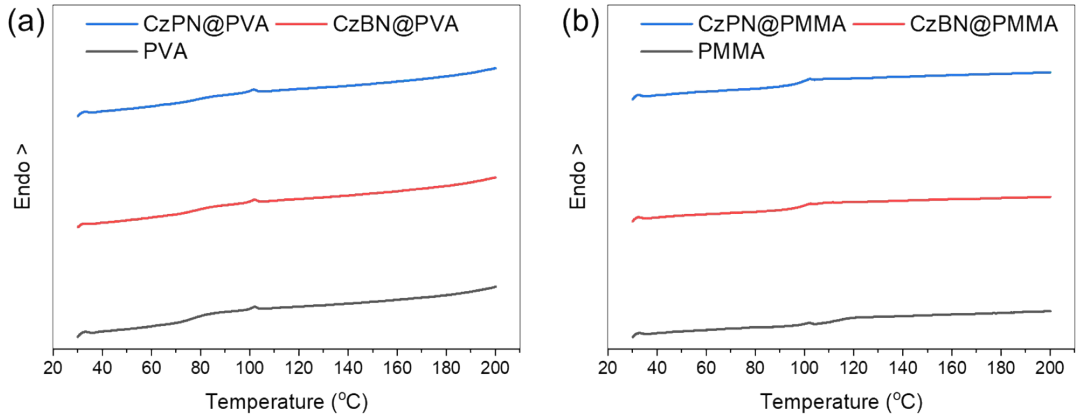

Figure S22 (a) DSC thermograms of CzBN@PVA, CzPN@PVA, PVA films. (b) DSC thermograms of CzBN@PMMA, CzPN@PMMA, PMMA films. The doping concentration of the films was 1 wt%.

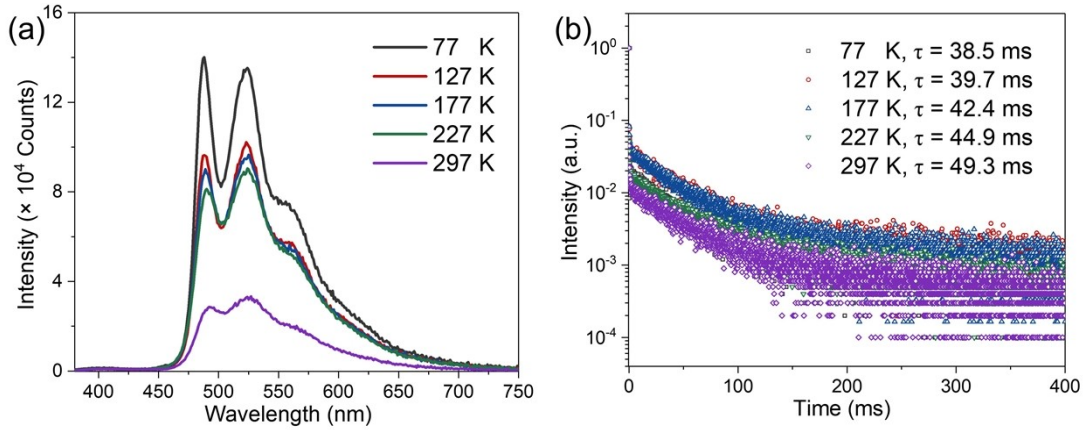

Figure S22 (a) Delayed PL spectra of CzBN@PVA films at different temperatures in air. (b) Time-resolved decay curves for the bands at 400 nm of CzBN@PVA films at different temperatures in air.

Table S2 The energy levels and transition configurations of CzPN revealed by TD-DFT calculations. The matched triplet excited states that contained the same orbital

transitions components of S_1 were marked in red.

Excited States	n-th	Energy (eV)	Transition configurations (%)
S_n	1	3.3439	H → L 98.0%
T_n	1	2.7328	H → L 61.8%, H-2 → L 15.3%
	2	3.2021	H-1 → L+2 54.7%, H-1 → L 10.2%, H → L+3 7.8%, H-2 → L+2 6.5%, H → L+2 5.5%
	3	3.3268	H → L+2 77.3%, H-1 → L 8.1%
	4	3.4409	H-1 → L 37.3%, H → L 21.8%, H-1 → L+2 10.7%, H → L+2 8.8%
	5	3.5177	H-1 → L 32.6%, H-3 → L 22.3%, H-2 → L 10.8%, H-3 → L+1 9.4%, H → L 8.0%, H-4 → L+1 5.1%
	6	3.5952	H → L+1 68.3%, H-1 → L+2 9.7%, H-2 → L+1 6.5%, H-3 → L 5.1%
	7	3.9494	H-4 → L 25.8%, H-3 → L 25.4%, H-2 → L 17.3%, H → L+3 10.1%, H-3 → L+1 7.6%
	8	4.0452	H → L+3 22.8%, H-1 → L+1 17.8%, H-2 → L+2 13.3%, H-1 → L+2 8.1%, H → L+4 7.1%, H-2 → L 5.9%

Table S3 The energy levels and transition configurations of CzBN revealed by TD-DFT calculations. The matched triplet excited states that contained the same orbital transitions components of S_1 were marked in red.

Excited States	n-th	Energy (eV)	Transition configurations (%)
S_n	1	3.7941	H → L 95.1%
T_n	1	2.9353	H → L 57.5%, H-2 → L 15.7%, H-1 → L+1 12.0%
	2	3.2402	H-1 → L+1 36.1%, H → L+1 31.9%, H-2 → L+1 7.2%
	3	3.3465	H → L+1 59.0%, H-1 → L+1 21.5%, H-1 → L 5.1%
	4	3.7660	H-1 → L 41.7%, H-1 → L+1 16.5%, H → L 16.1%, H → L+3 6.0%, H-4 → L 5.9%
	5	3.8519	H-1 → L 34.0%, H-2 → L 18.9%, H-4 → L 12.1%, H-3 → L+2 9.7%, H → L 5.7%, H → L+3 5.7%
	6	4.0803	H → L+3 26.8%, H-2 → L+1 14.9%, H → L+4 7.5%, H-1 → L+1 6.7%, H-2 → L+3 6.2%, H-1 → L 5.3%
	7	4.1660	H → L+2 55.5%, H-3 → L 20.4%, H-2 → L+2 12.6%
	8	4.3201	H → L+4 20.1%, H-2 → L 10.4%, H-1 → L+5 9.9%, H-2 → L+1 9.4%, H-5 → L+1 9.4%, H-2 → L+3 6.8%, H-4 → L+1 6.4%, H → L 6.2%

References

1. C. Lee, W. Yang and R. G. Parr, Development of the Colle-Salvetti correlation-energy formula into a functional of the electron density, *Phys. Rev. B*, 1988, **37**, 785-789.
2. P. J. Stephens, F. J. Devlin, C. F. Chabalowski and M. J. Frisch, Ab Initio Calculation of Vibrational Absorption and Circular Dichroism Spectra Using Density Functional Force Fields, *J. Chem. Phys.*, 1994, **98**, 11623-11627.
3. Y. Yang, Y. Liang, Y. Zheng, J.-A. Li, S. Wu, H. Zhang, T. Huang, S. Luo, C. Liu, G. Shi, F. Sun, Z. Chi and B. Xu, Efficient and Color-Tunable Dual-Mode Afterglow from Large-Area and Flexible Polymer-Based Transparent Films for Anti-Counterfeiting and Information Encryption, *Angew. Chem. Int. Ed.*, 2022, **61**, e202201820.
4. F. Neese, Software update: the ORCA program system, version 4.0, *WIREs Computational Molecular Science*, 2018, **8**, e1327.
5. W. Humphrey, A. Dalke and K. Schulten, VMD: Visual Molecular Dynamics, *J. Mol. Graph.*, 1996, **14**, 33-38.
6. T. Lu and F. Chen, Multiwfn: A Multifunctional Wavefunction Analyzer, *J. Comput. Chem.*, 2012, **33**, 580-592.